RESEARCH ARTICLE

Finite-Time Autonomous Vehicle Path Tracking Control Based on State Constraint

PENGXIANG LI[1], SUCAI ZHANG [ID]2, AND YAN LIU [ID]3

[1]School of Mechanical Engineering, Ningxia Institute of Science and Technology, Shizuishan 753000, China
[2]School of Mechanical Engineering and Automation, Northeastern University, Shenyang 110819, China
[3]School of Automobile and Traffic Engineering, Liaoning University of Technology, Jinzhou 121001, China

Corresponding author: Sucai Zhang (zhang_sucai@163.com)

ABSTRACT A finite-time path tracking control scheme with state constraint is proposed for the autonomous vehicle path tracking control problem affected by compound disturbance and unmeasurable variables. First, the state observer and the disturbance observer are constructed to estimate the sideslip angle and the compound disturbance, respectively. On this basis, the state constraint finite-time controller is designed by combining the finite-time technique with the introduction of the barrier Lyapunov function and the backstepping control technique. Stability analysis is carried out according to the Lyapunov stability theory to ensure that all signals of the closed-loop system are bounded in finite time. Finally, the effectiveness of the proposed method is demonstrated by simulation and hardware-in-the-loop (HIL) experiments.

INDEX TERMS Path tracking, observers, backstepping, barrier Lyapunov function, finite-time.

I. INTRODUCTION

In recent years, with the growth of the number of vehicles, traffic congestion and vehicle safety issues are becoming more and more prominent, and drivers are prone to fatigue during long periods of driving, which can lead to traffic accidents [1]. Therefore, autonomous vehicles have enormous potential in solving these problems and are receiving widespread attention from academia, industry, and government. Autonomous vehicle needs the fusion of multidisciplinary knowledge, including environment awareness system, decision planning system and motion control system. In general, motion control of autonomous vehicle can be achieved by longitudinal control and lateral control based on current vehicle state and road information. Longitudinal control maintains the vehicle at the desired speed and at a safe distance from the vehicle in front, mainly by controlling the brakes and accelerator. Lateral motion control focuses on tracking a reference path by adjusting the lateral position and orientation of the autonomous vehicle in different road environments. Therefore, path tracking control is an

The associate editor coordinating the review of this manuscript and approving it for publication was Yang Tang [ID].

important part and key technology of motion control system. This paper focuses on the path tracking control problem of autonomous vehicle.

Path tracking control is one of the key technologies for autonomous vehicle. In the literature [2], the authors developed a visual vehicle dynamics model based on computer vision algorithms and applied it to a real-time (RT) control task. In order to improve the effectiveness of the path tracking control, several control methods are used to design the path tracking controller, including full state feedback control feedforward control [3], proportional integral derivative (PID) control [4], fuzzy control [5], sliding mode control (SMC) [27], robust control [7] and model predictive control (MPC) [8]. In the last decades, in order to address the system uncertainties and external disturbance present in autonomous vehicle, as well as the problems of traditional methods (e.g., chatting in the control input of sliding mode control). Several innovative control methods are investigated, including observer-based control and artificial intelligence-based control (e.g., neural networks). In [9], designed a state observer and a disturbance observer to estimate the sideslip angle and unknown disturbance, respectively, and used a second-order sliding mode to solve

the chattering problem existing in the traditional sliding mode control. In recent years, MPC has been gradually used by scholars for path tracking control of autonomous vehicle, and it has been improved on the basis of traditional MPC by combining other control methods to improve the tracking accuracy. In [10], based on nonlinear MPC control, combined with vehicle steering and braking, the vehicle is made to perform obstacle avoidance path tracking, and the effectiveness of the method is verified by simulation and experiment. In [11], a linear MPC for autonomous vehicle is proposed, where the trajectory in finite horizon is known at each time step, and the reference trajectory is tracked by the MPC calculating the front wheel angle. In [12], a tire parameter online adaptive module is designed to compensate the model and preview distance is added to the MPC controller to improve the tracking accuracy. In [13], the use of Square Root Kalman Filter for real-time estimation of tire lateral force and correction of tire lateral stiffness improves the model's accuracy. This approach solves the problem of model uncertainty well, but needs to address the effect of unknown disturbance on the control accuracy. However, most of the algorithms rely on linear models. In practice, the sideslip angle of the linear model is difficult to obtain, and expensive instruments are needed to measure it. Moreover, model uncertainty and external disturbance are not taken into account. It can lead to reduced or even unstable path tracking accuracy of autonomous vehicles under complex working conditions. In addition, some algorithms such as MPC require hardware with high arithmetic power, which leads to high hardware cost and is difficult to use in practice.

The backstepping method is a systematic design method for systems with uncertain parameters, which has the advantages of convenient design and strong robustness. In recent years, it has been widely applied. The basic idea of designing controllers based on backstepping is to decompose complex nonlinear systems into subsystems that do not exceed the system order, and then design partial Lyapunov functions and intermediate virtual control variables for each subsystem, all the way back to the entire system, and design control laws. In [14] used radial basis function neural networks to approximate tire lateral stiffness based on the backstepping control method to compensate for the uncertainty of tire stiffness. The backstepping method is widely used in industrial control applications, such as steer by wire control [15], [16], fuel cell control [17], servo motor control [18], etc. However, the backstepping control method is seldom used in the path tracking control of autonomous vehicle. Although the backstepping method is robust and real-time, with good control accuracy. But in practice it is not possible to limit the tracking error to a given range. This may lead to loss of control of the vehicle during path tracking. In other fields of engineering applications, the barrier Lyapunov function approach has been widely studied and applied to solve such problems [19], [20], [21].

However, the barrier Lyapunov function only constrains the error to a certain range and does not consider the convergence rate of the tracking error. In the past few decades, the convergence rate of various systems has become an increasingly popular topic in the field of control. Finite time control and fixed time control have aroused the research interest of scholars because of their advantages of fast convergence rate, strong disturbance resistance and high control accuracy. The concept of finite-time control was introduced in [22] which allows the system to achieve control objectives at a fast rate within a finite time. In [23], for the distributed adaptive fixed-time platoon tracking problem, the singularity problem in fixed-time and finite-time control is well solved using inequality techniques and power transformation schemes instead of approximation methods. In [24], the proposed method is used for nonlinear multiagent systems by combining the fixed-time control with prescribed performance function to shorten the convergence time of the tracking error while limiting the tracking error, and significant control results are achieved. In [25], fixed-time control is combined with fault-tolerant control and applied to a class of switched nonlinear systems, and the effectiveness of the proposed strategy is verified by simulation. Inspired by the above literature, finite time control is added to improve the tracking error convergence rate and tracking accuracy while imposing state constraints on the tracking error.

Inspired by all discussions, for the autonomous vehicle path tracking problem affected by compound disturbance and measurable variables, this paper designs state observers and disturbance observer to estimate the sideslip angle and compound disturbance, respectively, and proposes path tracking controllers with state constraints, finit time control and proves the effectiveness of the proposed method through simulation and hardware-in-the-loop experiments. The main contributions of this paper are summarized as follows:

1) The state observer and disturbance observer designed in this paper can estimate the sideslip angle and the compound disturbance respectively, which improves the tracking accuracy. Saving the cost of autonomous vehicle by eliminating the need for expensive sensors to measure the sideslip angle.

2) Based on the backstepping method, the barrier Lyapunov function and finite time control technique are introduced to ensure that constraints are imposed on the system while shortening the convergence time of the tracking error, thus improving the path tracking accuracy of autonomous vehicle. It can ensure that the tracking error of autonomous vehicle is always within a certain range during the path tracking process, and at the same time the tracking error converges to zero very quickly. improves the stability of autonomous vehicle.

The rest of this paper is organized as follows. Section II develops the vehicle two-degree-of-freedom model and the tracking model and gives the relevant lemmas. The state observer and controller are designed and rigorously analysed for stability in Section III. In Section IV, the effectiveness of the proposed method is verified through simulation

and hardware-in-the-loop experiments. Finally, Section V concludes this paper.

II. VEHICLE DYNAMICS MODEL AND TRACKING MODEL
A. VEHICLE DYNAMICS MODEL

The vehicle is a complex nonlinear system and it is difficult to derive its exact model. In order to facilitate the design of the controller, the vehicle model is usually simplified to a two-degrees-of-freedom model with the following assumptions: 1) Neglecting the transfer of loads between the front and rear of the vehicle; 2) Assuming the body and suspension system are rigid systems; 3) Neglecting the effects of friction and damping in the steering system. The schematic diagram of the two-degrees-of-freedom model of the vehicle is shown in Fig. 1.
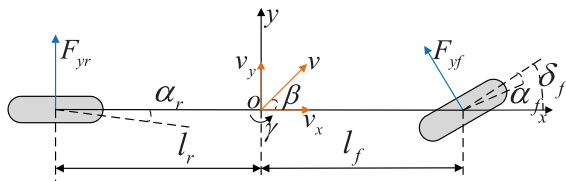

FIGURE 1. The sketch of vehicle two degrees of freedom model.

In Fig. 1, v_x is the longitudinal velocity; v_y is the lateral velocity; β is the sideslip angle; γ is the yaw rate; δ_f is the front wheel angle.

The two degrees of freedom dynamic equation of the vehicle is as follows:

$$\begin{cases} \dot{\beta} = \dfrac{F_{yf} + F_{yr}}{mv_x} - \gamma + d_1 \\ \dot{\gamma} = \dfrac{l_f F_{yf} - l_r F_{yr}}{I_z} + d_2 \end{cases} \quad (1)$$

where, m is the mass of the vehicle; I_z is the moment of inertia around the z-axis; l_f and l_r denote the distance from the center of mass to the front and rear axes, respectively; d_1 and d_2 denote the compound disturbance; F_{yf} and F_{yr} are the lateral force on the front and rear wheels, respectively.

Considering some non-linear characteristics of tires with complex structures, the brush tyre model is used to simulate the tire lateral forces. At the same time, in order to facilitate the analysis of the vehicle system, appropriate simplifications are made, and the lateral force equations of the brush tyre model are shown below:

$$\begin{cases} F_y = -C_\alpha \dfrac{\tan \alpha}{(1+\kappa)f} F \\ F = f - \dfrac{1}{3\mu F_z} f^2 + \dfrac{1}{27\mu^2 F^2} f^3, \ f \le 3\mu F_z \\ F = \mu F_z, \ otherwise \\ f = \sqrt{C_\alpha^2 \left(\dfrac{\kappa}{1+\kappa}\right)^2 + C_\alpha^2 \left(\dfrac{\tan \alpha}{1+\kappa}\right)^2} \\ \kappa = \dfrac{R_\omega \omega_\omega - V_{\omega x}}{V_{\omega x}} \end{cases} \quad (2)$$

where, C_α is the tire lateral stiffness; α is the slip angle; μ is the maximum road adhesion coefficient; F_z is the tire vertical force; R is the tire radius; w is the tire angular velocity; κ is the tire slip rate; v_x is the tire longitudinal velocity.

Since this paper assumes constant vehicle speed, it can be obtained that $Rw \approx v_x$. The tyre lateral deflection stiffness is related to the load and the road surface adhesion coefficient, however, the vehicle load does not vary much at a constant speed. Therefore, the tire lateral deflection stiffness is assumed to be constant. The lateral force equation is simplified as follows:

$$f_{coupled}(\alpha, F_z) = \begin{cases} -C_\alpha \tan \alpha + \Gamma, & |\alpha| < \arctan(\dfrac{3\mu F_z}{C_\alpha}) \\ -\mu F_z \text{sign} \alpha, & otherwise \end{cases} \quad (3)$$

where, $\Gamma = \dfrac{C_\alpha^2}{3\mu F_z} |\tan \alpha| \tan \alpha - \dfrac{C_\alpha^3}{27\mu^2 F_z^2} \tan^3 \alpha$.

The lateral forces on the front and rear tires can be expressed as:

$$\begin{cases} F_{yf} = f_{coupled}(\alpha_f, F_{zf}) \\ F_{yr} = f_{coupled}(\alpha_r, F_{zr}) \end{cases} \quad (4)$$

where, F_{zf} and F_{zr} are the vertical forces on the front and rear tires respectively.

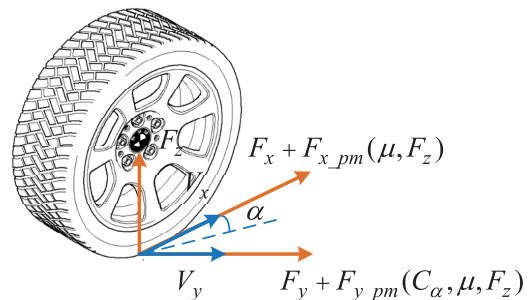The sketch of the force structure of a tire is shown in Fig. 2.

FIGURE 2. The sketch of the force structure of tire.

In Fig. 2, $F_{x\_pm}(\mu, F_z)$ and $F_{y\_pm}(\mu, F_z)$ are the longitudinal and lateral forces due to changes in road conditions. Due to the assumption of constant vehicle velocity, the variation of tire lateral deflection angle is kept within a small range, and the tire lateral deflection angle is assumed to be small, resulting in a lateral force:

$$\begin{cases} F_{yf} = -C_{\alpha f}\alpha_f + F_{yf-um} \\ F_{yr} = -C_{\alpha r}\alpha_r + F_{yr-um} \end{cases} \quad (5)$$

where, $C_{\alpha f}$ and $C_{\alpha r}$ are the front and rear tire lateral deflection stiffness respectively; $F_{HOT}(\alpha_f)$ and $F_{HOT}(\alpha_r)$ are the higher-order terms in the front and rear wheel lateral forces, respectively; F_{yf-um} and F_{yr-um} are the total unmodelled lateral force in the front and rear wheel, respectively.

The front and rear wheel slip angle is linearised as follows:

$$\begin{cases} \alpha_f(t) \approx \beta + \dfrac{l_f \gamma}{V_x} - \delta_f \\ \alpha_r(t) \approx \beta - \dfrac{l_r \gamma}{V_x} \end{cases} \tag{6}$$

Substituting (5) and (6) into (1) yields:

$$\begin{cases} \dot{\beta} = -\dfrac{C_{\alpha f} + C_{\alpha r}}{m v_x} \beta - \left(\dfrac{C_{\alpha f} l_f - C_{\alpha r} l_r}{m v_x^2} + 1 \right) \gamma + \dfrac{C_{\alpha f}}{m v_x} \delta_f + D_1 \\ \dot{\gamma} = -\dfrac{C_{\alpha f} l_f - C_{\alpha r} l_r}{I_z} \beta - \dfrac{C_{\alpha f} l_f^2 + C_{\alpha r} l_r^2}{I_z v_x} \gamma + \dfrac{C_{\alpha f} l_f}{I_z} \delta_f + D_2 \end{cases} \tag{7}$$

where, $D_1 = d_1 + \frac{1}{m v_x}(F_{yf-um} + F_{yr-um})$; $D_2 = d_2 + \frac{1}{I_z}(l_f F_{yf-um} - l_r F_{yr-um})$.

Remark 1: The compound disturbance $D_i (i = 1, 2)$ needs to satisfy the following conditions: $D_i \leq D_{i\max}, \dot{D}_i \leq \overline{D}_i$. From the point of view of practical engineering applications, $d_i (i = 1, 2)$ is mainly the external disturbance during vehicle driveing, such as disturbance by lateral winds, etc., which are bounded in practice by the existence of an unknown maximum value. The velocity and acceleration of the vehicle are bounded in practice and the maximum value is related to the performance of the vehicle. The tire force in the unmodelled part of the vehicle tire is related to the vehicle loads and road conditions, and in the actual driving process of the vehicle, there are small changes in the road and vehicle loads, and there is an unknown maximum value for the tire force in the unmodelled part of the vehicle tire. Therefore, there exists unknown $D_{i\max}$ and $\overline{D}_i$ meet $D_i \leq D_{i\max}$ and $\dot{D}_i \leq \overline{D}_i$.

B. TRACKING MODEL

In general, path tracking control is to make the vehicle track the reference path by controlling the front wheel angle so that the error between the vehicle position and the reference path is reduced to zero. Therefore, a vehicle path tracking model is established to describe the relationship between the vehicle position and the reference path as shown in Fig. 3.
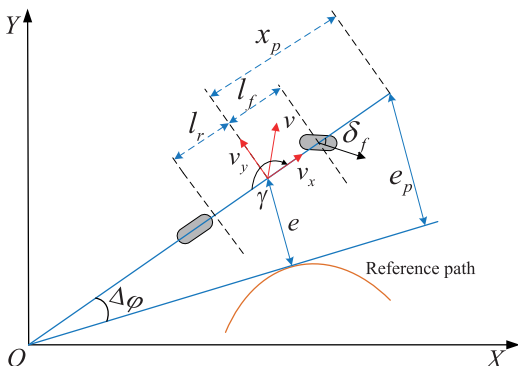

FIGURE 3. The sketch of the structure of the path tracking model.

In Fig. 3, e is the error between the center of mass of the vehicle and the reference path; $\Delta\varphi$ is the yaw error; Then it is difficult to control e and $\Delta\varphi$ to be zero at the same time for a front wheel steering vehicle. Therefore, an alternative approach is to combine e and $\Delta\varphi$ at a distance x_p in front of the vehicle to obtain a new error e_p so that e_p is zero. Define the error dynamics equation as follows [3]:

$$\begin{cases} \dot{e} = v_y \cos(\Delta\varphi) + v_x \sin(\Delta\varphi) \\ \dot{s} = v_x \cos(\Delta\varphi) - v_x \sin(\Delta\varphi) \\ e_p = e + x_p \sin(\Delta\varphi) \\ \Delta\varphi = \varphi_o - \varphi_d \end{cases} \tag{8}$$

where, s is the distance along the reference path; x_p is the projection distance; φ_o is the yaw angle; φ_d is the reference yaw angle.

Small angle assumptions are made to obtain $\cos(\Delta\varphi) \approx 1$, $\sin(\Delta\varphi) \approx \Delta\varphi$ and derivation of (8) is obtained:

$$\begin{cases} \dot{e} = v_y + v_x \Delta\varphi \\ \dot{e}_p = \dot{e} + x_p \Delta\dot{\varphi} \\ e_p = e + x_p \Delta\varphi \\ \Delta\dot{\varphi} = \dot{\varphi}_o - \dot{\varphi}_d = \gamma - K\dot{s} \end{cases} \tag{9}$$

where, K is the curvature of the reference path.

Derivation for $\dot{e}, \dot{e}_p, \Delta\dot{\varphi}$ is obtained:

$$\begin{cases} \ddot{e} = \dot{v}_y + \dot{v}_x \Delta\varphi + v_x \Delta\dot{\varphi} \\ \Delta\ddot{\varphi} = \dot{\gamma} - \dot{K}\dot{s} - K\ddot{s} \\ \ddot{e}_p = \ddot{e} + x_p \Delta\ddot{\varphi} \\ \quad = \dot{v}_y + \dot{v}_x \Delta\varphi + v_x(\gamma - K\dot{s}) + x_p(\dot{\gamma} - \dot{K}\dot{s} - K\ddot{s}) \end{cases} \tag{10}$$

Substituting (7) into (10) yields:

$$\ddot{e}_p = x_p(-\dot{K}\dot{s} - K\ddot{s}) + x_p \left(-\dfrac{aC_{\alpha f} - bC_{\alpha r}}{I_z} \beta - \dfrac{a^2 C_{\alpha f} + b^2 C_{\alpha r}}{I_z v_x} \gamma \right. $$
$$\left. + \dfrac{aC_{\alpha f}}{I_z} \delta_f + D_2 \right) \dot{v}_y + \dot{v}_x \Delta\varphi + v_x(\gamma - K\dot{s}) \tag{11}$$

Rewriting (11) as a state space equation takes the following form:

$$\begin{cases} \dot{\xi}_1 = \xi_2 \\ \dot{\xi}_2 = \zeta_1 + \zeta_2 + \zeta_3 u + x_p D_2 \end{cases} \tag{12}$$

where, $\xi_1 = e_p, \xi_2 = \dot{e}_p, \zeta_1 = \dot{v}_y + \dot{v}_x \Delta\varphi + v_x(\gamma - K\dot{s}), \zeta_2 = x_p(a_{21}\beta + a_{22}\gamma - \dot{K}\dot{s} - K\ddot{s}), \zeta_3 = b_2 x_P, a_{21} = -\dfrac{aC_{\alpha f} - bC_{\alpha r}}{I_z}, a_{22} = -\dfrac{a^2 C_{\alpha f} + b^2 C_{\alpha r}}{I_z v_x}, b_2 = \dfrac{aC_{\alpha f}}{I_z}, u = \delta_f$.

Lemma 1 [26]: For any $(x, y) \in R^2$, the following Young's inequality satisfies:

$$xy \leq \dfrac{\varpi^p}{p}|x|^p + \dfrac{1}{q\varpi^q}|y|^q \tag{13}$$

where, $\varpi > 0, p > 1$ and $q > 1$, are constants satisfying that $(q - 1)(p - 1) = 1$.

Lemma 2 [27]: Suppose there exists a positive definite function $V(z)$ and $a > 0, b > 0, \lambda \in (0, b), \tau \in (0, 1)$.

For a nonlinear system $\dot{z} = f(z)$, there exits $\dot{V}(z) + aV^\tau(z) + bV(z) - C \leq 0$. Then it follows that $\dot{z} = f(z)$ is practically finite time stable, satisfying $V(z) \leq \frac{C}{b-\lambda}$ and setting time $T_r = t_0 + \frac{1}{\lambda(1-\tau)} \ln \frac{V^{1-\tau}(t_0) + \frac{a}{\lambda}}{\frac{C}{(b-\lambda)b}^{1-\tau} + \frac{a}{\lambda}}$.

Remark 2: In recent literature, there are two main classical finite time stability theories for the system $\dot{x} = f(x)$ [27]: 1) Selecting V (x) as the Lyapunov function, if $V(x)$ satisfies $\dot{V}(x) \leq aV^\gamma(x)(a > 0, 0 < \gamma < 1)$ along the derivative of the system, then the system is called to be finite time stability. However, when $V(x) \gg 1$, it means that $0 \ll V^\gamma(x) \ll V(x)$, at which point the rate of convergence of the system depends largely on the level of exponential growth. 2) Thus, a type of stability known as fast finite time stability was devised, denoted as $\dot{V}(x) + bV(x) + aV^\gamma(x) \leq 0$. As expressed in [27], when the above two finite-time stability theories are applied in combination with a universal approximator (e.g., neural network or fuzzy logic system), the system may enter into a neighborhood near the origin and always fails to arrive at the origin because of the fact that the universal approximator always has a certain approximation error. Consequently, the finite time stability technique capable of dealing with redundant terms (e.g., approximation errors) is referred to as practical finite time stability, denoted as $\dot{V}(x) + bV(x) + aV^\gamma(x) - \eta \leq 0$. A detailed proof of this can be found in [27], and this formulation can also be found in the following literature: Corollary 1 in [28]; Lemma 2 in [29]; Corollary 1 in [30]; and Lemma 2.1 in [31]. A similar notion is finite time bounded, in [32], the time-varying system $\dot{x}(t) = A(t)x(t) + G(t)w, t \in [0, T]$ is defined. For any w satisfying $w^T w \leq d, d \geq 0$, there exists $c_2 > c_1, R > 0$ such that $x^T(0)Rx(0) \leq c_1 \Rightarrow x^T(t)Rx(t) < c_2, \forall t \in [0, T]$, then the system is said to be finite time bounded.

Lemma 3 [28]: For variables θ and Γ, there exist positive constants ρ, ℓ and Π with the following inequality:

$$|\theta|^\rho |\Gamma|^\ell \leq \frac{\rho}{\rho + \ell} \Pi |\theta|^{\rho + \ell} + \frac{\ell}{\rho + \ell} \Pi^{-\frac{\rho}{\ell}} |\Gamma|^{\rho + \ell} \quad (14)$$

III. OBSERVER AND CONTROLLER DESIGN
A. OBSERVER DESIGN

The sideslip angle represents the angle between the direction of the vehicle's centre of mass velocity and the vehicle's longitudinal axis. This angle directly reflects the degree of non-linearity of the vehicle motion and the steering following characteristics, as well as the utilisation of the vehicle's lateral attachment. At the low speed of the vehicle, the effect of the sideslip angle can be ignored. And when the vehicle is travelling at high speed, the vehicle will be in an unstable state if the steering angle is too large, which will lead to the increase of the sideslip angle. Therefore, the sideslip is an important parameter to characterize the stability of vehicle. Whereas in practice it needs to be measured by expensive sensors which will lead to increase in the cost of the vehicle. So, an observer is used to get the estimated value of sideslip angle while saving costs.

According to (7), it can be seen that sideslip angle and yaw rate are state variables, and the state observer is designed to estimate the state variables. In practice, the yaw rate can be measured by the Inertial Measurement Unit (IMU) built into the Differential Global Positioning System (DGPS), and the yaw rate is selected as the system output. However, due to the low accuracy of selecting only one variable as the system output to design the observer, in order to improve the estimation accuracy of the state observer, lateral acceleration is added as the system output. Lateral acceleration can also be measured by the IMU, and lateral acceleration is expressed as:

$$a_y = -\frac{C_{\alpha f} + C_{\alpha r}}{m} \beta - \frac{aC_{\alpha f} - bC_{\alpha r}}{mv_x} \gamma + \frac{C_{\alpha f}}{m} \delta_f \quad (15)$$

According to (7) and (15) the following nonlinear system form is obtained:

$$\begin{cases} \dot{X} = (A - LC)X + (B - LE)u + D + LY \\ Y = CX + Eu \end{cases} \quad (16)$$

where,

$$X = [x_1, x_2]^T = [\beta, \gamma]^T, \quad Y = [a_y, \gamma]^T,$$
$$C = \begin{bmatrix} v_x a_{11} & v_x(a_{12} + 1) \\ 0 & 1 \end{bmatrix}, \quad B = \begin{bmatrix} b_1 \\ b_2 \end{bmatrix},$$
$$L = \begin{bmatrix} L_{11} & L_{12} \\ L_{21} & L_{22} \end{bmatrix}, \quad A = \begin{bmatrix} a_{11} & a_{12} \\ a_{21} & a_{22} \end{bmatrix},$$
$$E = \begin{bmatrix} v_x b_1 \\ 0 \end{bmatrix}, \quad D = \begin{bmatrix} D_1 \\ D_2 \end{bmatrix},$$
$$a_{11} = -\frac{C_{\alpha f} + C_{\alpha r}}{mv_x}, \quad a_{12} = -(\frac{aC_{\alpha f} - bC_{\alpha r}}{mv_x^2} + 1),$$
$$a_{21} = -\frac{aC_{\alpha f} - bC_{\alpha r0}}{I_z}, a_{22} = -\frac{a^2 C_{\alpha f} + b^2 C_{\alpha r}}{I_z v_x},$$
$$b_1 = \frac{C_{\alpha f}}{mv_x}, b_2 = \frac{aC_{\alpha f}}{I_z}, u = \delta_f.$$

Define $H = A - LC$ and select the appropriate L such that H satisfies Herwitz, choosing the Lyapunov equation:

$$H^T P + PH = -Q \quad (17)$$

where, $P \in R^+$ and $Q \in R^+$ with $P = P^T$ and $Q = Q^T$.

Design the state observer as follows:

$$\begin{cases} \dot{\hat{X}} = (A - LC)\hat{X} + (B - LE)u + \hat{D} + LY \\ \hat{Y} = C\hat{X} + Eu \end{cases} \quad (18)$$

where, $\hat{X} = [\hat{x}_1, \hat{x}_2]^T$ is the estimate of X; $\hat{Y} = [\hat{a}_y, \hat{\gamma}]^T$ is the estimate of Y; $\hat{D} = [\hat{D}_1, \hat{D}_2]^T$ is the estimate of D.

Define the auxiliary variable $\hat{\lambda}_i = \hat{D}_i - \gamma_i \hat{x}_i$, $i = 1, 2$. The disturbance observer is designed as:

$$\begin{cases} \hat{D}_i = \hat{\lambda}_i + \gamma_i \hat{x}_i \\ \dot{\hat{\lambda}}_i = -\gamma_i(b_i u + a_{i1}\hat{x}_1 + a_{i2}\hat{x}_2 + \hat{\lambda}_i + \gamma_i \hat{x}_i) \end{cases} \quad (19)$$

where, γ_i is the designed constant. Define $\tilde{\lambda}_i = \lambda_i - \hat{\lambda}_i$, $\dot{\tilde{\lambda}}_i = \dot{\lambda}_i - \dot{\hat{\lambda}}_i$. According to Lemma 1, it can be concluded that:

$$
\begin{cases}
\tilde{\lambda}_i \gamma_i a_{ii} \tilde{x}_i \leq \dfrac{\epsilon_{1i}}{2} \tilde{\lambda}_i^2 + \dfrac{1}{2\epsilon_{1i}} \gamma_i^2 a_{ii}^2 \tilde{X}^T \tilde{X} \\[2mm]
\tilde{\lambda}_i \dot{D}_i \leq \dfrac{\epsilon_{2i}}{2} \tilde{\lambda}_i^2 + \dfrac{1}{2\epsilon_{2i}} \bar{D}_i^2 \\[2mm]
\gamma_i^2 \tilde{\lambda}_i \tilde{x}_i \leq \dfrac{\epsilon_{3i}}{2} \tilde{\lambda}_i^2 + \dfrac{1}{2\epsilon_{3i}} \gamma_i^4 \tilde{X}^T \tilde{X} \\[2mm]
\tilde{\lambda}_1 \gamma_1 a_{12} \tilde{x}_2 \leq \dfrac{\epsilon_{41}}{2} \tilde{\lambda}_1^2 + \dfrac{1}{2\epsilon_{41}} \gamma_1 a_{12}^2 \tilde{X}^T \tilde{X} \\[2mm]
\tilde{\lambda}_2 \gamma_2 a_{21} \tilde{x}_1 \leq \dfrac{\epsilon_{42}}{2} \tilde{\lambda}_2^2 + \dfrac{1}{2\epsilon_{42}} \gamma_2 a_{21}^2 \tilde{X}^T \tilde{X} \\[2mm]
\tilde{X}^T P \tilde{D}_i \leq \left(\dfrac{\epsilon_{5i}}{2} \|P\|^2 + \dfrac{1}{\epsilon_{5i}} \gamma_i^2 \right) \tilde{X}^T \tilde{X} + \dfrac{1}{\epsilon_{5i}} \tilde{\lambda}_i^2
\end{cases}
\tag{20}
$$

where, $\epsilon_{ji} \in R^+ (I = 1, 2, J = 1, \ldots, 5)$ is the designed constants.

Considering the following Lyapunov function:

$$
V_1 = \frac{1}{2} \tilde{X}^T P \tilde{X} + \sum_{i=1}^{2} \frac{1}{2} \tilde{\lambda}_i^2
\tag{21}
$$

The first order derivative of V_1 with respect to time is:

$$
\dot{V}_1 = \frac{1}{2} \dot{\tilde{X}}^T P \tilde{X} + \frac{1}{2} \tilde{X}^T P \dot{\tilde{X}} + \sum_{i=1}^{2} \tilde{\lambda}_i \dot{\tilde{\lambda}}_i
\tag{22}
$$

Substituting into equations (16), (18), (19) and (20) yields:

$$
\begin{aligned}
\dot{V}_1 \leq & -\left[\frac{1}{2} \lambda_{\min}(Q) - \sum_{i=1}^{2} \frac{\epsilon_{5i}}{2} \|P\|^2 - \sum_{i=1}^{2} \frac{1}{2\epsilon_{3i}} \gamma_i^4 - \sum_{i=1}^{2} \frac{1}{\epsilon_{5i}} \gamma_i^2 \right. \\
& \left. - \sum_{i=1}^{2} \frac{1}{2\epsilon_{1i}} \gamma_i^2 a_{ii}^2 - \frac{1}{2\epsilon_{41}} \gamma_1^2 a_{12}^2 - \frac{1}{2\epsilon_{42}} \gamma_2^2 a_{21}^2 \right] \tilde{X}^T \tilde{X} \\
& - \sum_{i=1}^{2} \left(\gamma_i - \sum_{j=1}^{4} \frac{\epsilon_{ji}}{2} - \frac{1}{\epsilon_{5i}} \right) \tilde{\lambda}_i^2 + \sum_{i=1}^{2} \frac{1}{2\epsilon_{2i}} \bar{D}_i^2
\end{aligned}
\tag{23}
$$

where, $\lambda_{\min}(Q)$ is the minimum eigenvalue of Q; $\kappa_1 = \frac{1}{2} \lambda_{\min}(Q) - \sum_{i=1}^{2} \frac{\epsilon_{5i}}{2} \|P\|^2 - \sum_{i=1}^{2} \frac{1}{2\epsilon_{3i}} \gamma_i^4 - \sum_{i=1}^{2} \frac{1}{\epsilon_{5i}} \gamma_i^2 - \sum_{i=1}^{2} \frac{1}{2\epsilon_{1i}} \gamma_i^2 a_{ii}^2 - \frac{1}{2\epsilon_{41}} \gamma_1^2 a_{12}^2 - \frac{1}{2\epsilon_{42}} \gamma_2^2 a_{21}^2$; $\kappa_{2i} = \gamma_i - \sum_{j=1}^{4} \frac{\epsilon_{ji}}{2} - \frac{1}{\epsilon_{5i}}$; $\kappa_3 = \sum_{i=1}^{2} \frac{1}{2\epsilon_{2i}} \bar{D}_i^2$.

According to (23), if $\kappa_1 > 0$, $\kappa_2 > 0$ and κ_3 is bounded, the estimation error $\tilde{X}$ is bounded according to Lyapunov stability theory. Therefore, this paper ensures that the state of the closed-loop system is bounded by designing an appropriate control method.

Remark 3: There are many observer design methods, such as the state observer proposed in the literature [25] and [33], which is able to have high estimation accuracy for unknown variables, especially when combined with Butterworth low-pass filter in [25] to further improve the estimation accuracy. In comparison, the state observer proposed in this paper has a simple structure and slightly lower tracking accuracy. However, considering that the team is currently building a real vehicle platform for autonomous vehicle, the proposed observers will be verified on the real

vehicle platform in the future work. The state observer proposed in this paper has a simple structure but is easy to adjust the design parameters and incorporates a disturbance observer, which may be more convenient to be verified in future experiments on real vehicle. Of course, in future work, we will also explore the application of other state observers (e.g., those proposed in [25] and [33]) in real-vehicle experiments to explore the advantages and disadvantages of different observers.

B. CONTROLLER DESIGN

In order to improve the path tracking accuracy, an barrier Lyapunov function is used on the basis of the traditional backstepping control method, and boundary parameters are set for the error. The proposed controller design is divided into two steps.

Step 1: Define the variable: $z_1 = \xi_1 - \xi_d$, $z_2 = \xi_2 - \eta_1$, since ξ_1 is the new tracking error after the tracking error is converted with the yaw angle error, and the purpose of the path tracking control of the autonomous vehicle is to make the tracking error converge to zero. Therefore, the desired tracking error of the tracking error should be zero, that is $\xi_d = 0$, $z_1 = \xi_1$. Selecting barrier Lyapunov function:

$$
V_2 = \frac{1}{2} \ln \frac{k_1^2}{k_1^2 - z_1^2}
\tag{24}
$$

Design virtual controller η_1:

$$
\eta_1 = -\varrho_1 z_1 - \frac{\varsigma_1 z_1^\tau}{(k_1^2 - z_1^2)^{\frac{\tau-1}{2}}} - \frac{z_1}{2(k_1^2 - z_1^2)}
\tag{25}
$$

where, k_1 is boundary parameter; ϱ_1 and ς_1 are constants; $\tau \in (0, 1)$.

Taking the derivative of V_2 and substituting (25) into (24) yields:

$$
\begin{aligned}
\dot{V}_2 &= \frac{z_1 \dot{z}_1}{k_1^2 - z_1^2} = \frac{z_1(z_2 + \alpha_1)}{k_1^2 - z_1^2} \\
&= \frac{z_1}{k_1^2 - z_1^2} \left(z_2 - \varrho_1 z_1 - \frac{\varsigma_1 z_1^\tau}{(k_1^2 - z_1^2)^{\frac{\tau-1}{2}}} - \frac{z_1}{2(k_1^2 - z_1^2)} \right) \\
&= \frac{z_1 z_2}{k_1^2 - z_1^2} - \frac{\varrho_1 z_1^2}{k_1^2 - z_1^2} - \frac{\varsigma_1 z_1^{\tau+1}}{(k_1^2 - z_1^2)^{\frac{\tau+1}{2}}} - \frac{z_1^2}{2(k_1^2 - z_1^2)^2}
\end{aligned}
\tag{26}
$$

According to Lemma 1, it can be concluded that:

$$
\frac{z_1 z_2}{k_1^2 - z_1^2} \leq \frac{z_1^2}{2(k_1^2 - z_1^2)^2} + \frac{1}{2} z_2^2
\tag{27}
$$

Substituting (27) into (26) yields:

$$
\dot{V}_2 \leq -\frac{\varrho_1 z_1^2}{k_1^2 - z_1^2} - \frac{\varsigma_1 z_1^{\tau+1}}{(k_1^2 - z_1^2)^{\frac{\tau+1}{2}}} + \frac{1}{2} z_2^2
\tag{28}
$$

Step 2: Selecting the barrier Lyapunov function:

$$
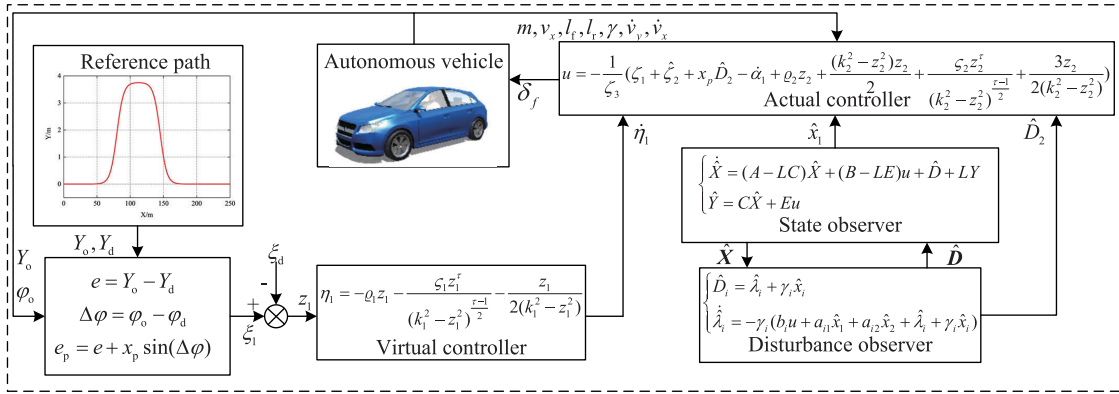V_3 = \frac{1}{2} \ln \frac{k_2^2}{k_2^2 - z_2^2}
\tag{29}
$$

FIGURE 4. The schematic structure of the proposed control method in this paper.

The controller u is designed as follows:

$$u = -\frac{1}{\zeta_3}(\zeta_1 + \hat{\zeta}_2 + x_p\hat{D}_2 - \dot{\alpha}_1 + \varrho_2 z_2 + \frac{(k_2^2 - z_2^2)z_2}{2}$$
$$+ \frac{\varsigma_2 z_2^\tau}{(k_2^2 - z_2^2)^{\frac{\tau-1}{2}}} + \frac{3z_2}{2(k_2^2 - z_2^2)}) \qquad (30)$$

where, k_2 is boundary parameter; ϱ_2 and ς_2 are constants; $\hat{\zeta}_2 = x_p(a_{21}\hat{\beta} + a_{22}\gamma - K\dot{s} - K\ddot{s})$.

Combining the state observer (18), the controller u, and the derivation of V_3 yields:

$$\dot{V}_3 = \frac{z_2}{k_2^2 - z_2^2}(x_p a_{21}\tilde{x}_1 + x_p(\tilde{\lambda}_2 + \gamma_2\tilde{x}_2) - \varrho_2 z_2 - \frac{z_2(k_2^2 - z_2^2)}{2}$$
$$- \frac{\varsigma_2 z_2^\tau}{(k_2^2 - z_2^2)^{\frac{\tau-1}{2}}} - \frac{3z_2}{2(k_2^2 - z_2^2)}) \qquad (31)$$

According to Lemma 1, it can be concluded that:

$$\begin{cases} \frac{z_2}{k_2^2 - z_2^2}x_p a_{21}\tilde{x}_1 \leq \frac{z_2^2}{2(k_2^2 - z_2^2)^2} + \frac{1}{2}x_p^2 a_{21}^2 \tilde{X}^T\tilde{X} \\ \frac{z_2}{k_2^2 - z_2^2}x_p\tilde{\lambda}_2 \leq \frac{z_2^2}{2(k_2^2 - z_2^2)^2} + \sum_{i=1}^2 \frac{1}{2}x_p^2\tilde{\lambda}_i^2 \\ \frac{z_2}{k_2^2 - z_2^2}x_p\gamma_2\tilde{x}_2 \leq \frac{z_2^2}{2(k_2^2 - z_2^2)^2} + \frac{1}{2}x_p^2\gamma_2^2\tilde{X}^T\tilde{X} \end{cases} \qquad (32)$$

Substituting (32) into (31) gives:

$$\dot{V}_3 \leq -\frac{\varrho_2 z_2^2}{k_2^2 - z_2^2} - \frac{1}{2}z_2^2 - \frac{\varsigma_2 z_2^{\tau+1}}{(k_2^2 - z_2^2)^{\frac{\tau+1}{2}}} + \sum_{i=1}^2 \frac{1}{2}x_p^2\tilde{\lambda}_i^2$$
$$+ (\frac{1}{2}x_p^2 a_{21}^2 + \frac{1}{2}x_p^2\gamma_2^2)\tilde{X}^T\tilde{X} \qquad (33)$$

C. STABILITY ANALYSIS

Theorem 1: For the path tracking model (12) with state observer (18) and disturbance observer (19), virtual controller (25) and controller (30), then all signals of the closed-loop system are bounded.

Proof 1 (Proof of Theorem 1): According to Lemma 3, it can be concluded that:

$$\begin{cases} (\frac{\lambda_{\min}(Q)\tilde{X}^T\tilde{X}}{4})^{\frac{\tau+1}{2}} \leq \frac{\lambda_{\min}(Q)}{4}\tilde{X}^T\tilde{X} + \frac{1-\tau}{2}(\frac{2}{\tau+1})^{-\frac{1+\tau}{1-\tau}} \\ (\frac{1}{2}\tilde{\lambda}_i^2)^{\frac{\tau+1}{2}} \leq \frac{1}{2}\tilde{\lambda}_i^2 + \frac{1-\tau}{2}(\frac{2}{\tau+1})^{-\frac{1+\tau}{1-\tau}} \end{cases} \qquad (34)$$

The Lyapunov function $V = V_1 + V_2 + V_3$ is chosen and can be obtained through (23), (28), (33) and (34):

$$\dot{V} \leq -C_1\frac{1}{2}\tilde{X}^T P\tilde{X} - \sum_{i=1}^2 C_{2i}\frac{1}{2}\tilde{\lambda}_i^2 - C_3\sum_{i=1}^2 \frac{1}{2}\frac{z_i^2}{k_i^2 - z_i^2}$$
$$- C_4(\frac{1}{2}\tilde{X}^T P\tilde{X})^{\frac{\tau+1}{2}} - C_5\sum_{i=1}^2 (\frac{1}{2}\tilde{\lambda}_i^2)^{\frac{\tau+1}{2}}$$
$$- C_6\sum_{i=1}^2 (\frac{1}{2}\frac{z_i^2}{k_i^2 - z_i^2})^{\frac{\tau+1}{2}} + C_0 \qquad (35)$$

where, $C_1 = -\frac{2}{\lambda_{\max}(P)}[\frac{1}{2}\lambda_{\min}(Q) - \sum_{i=1}^2 \frac{\epsilon_{5i}}{2}\|P\|^2 - \sum_{i=1}^2 \frac{1}{2\epsilon_{3i}}\gamma_i^4 - \sum_{i=1}^2 \frac{1}{\epsilon_{5i}}\gamma_i^2 - \sum_{i=1}^2 \frac{1}{2\epsilon_{1i}}\gamma_i^2 a_{ii}^2 - \frac{1}{2\epsilon_{41}}\gamma_1^2 a_{12}^2 - \frac{1}{2\epsilon_{42}}\gamma_2^2 a_{21}^2 - \frac{1}{2}x_p^2 a_{21}^2 - \frac{1}{2}x_p^2\gamma_2^2]$, $C_{2i} = 2(\gamma_i - \sum_{j=1}^4 \frac{\epsilon_{ji}}{2} - \frac{1}{\epsilon_{5i}}) - 1$, $C_3 = 2\min\{\varrho_1, \varrho_2\}$, $C_4 = (\frac{\lambda_{\min}(Q)}{2\lambda_{\max}(P)})^{\frac{\tau+1}{2}}$, $C_5 = 1$, $C_6 = 2^{\frac{\tau+1}{2}}\min\{\varsigma_1, \varsigma_2\}$, $C_0 = \sum_{i=1}^2 \frac{1}{2\epsilon_{2i}}\bar{D}_i^2 + (1-\tau)(\frac{2}{\tau+1})^{-\frac{1+\tau}{1-\tau}}$.

Define the compact set $\Omega_z = \{z_i | |z_i| \leq k_i, i = 1, 2\}$, then on Ω_z, it follows [34]: $\ln\frac{k_i^2}{k_i^2 - z_i^2} \leq \frac{z_i^2}{k_i^2 - z_i^2}$, (35) is expressed as:

$$\dot{V} \leq -aV - bV^{\frac{\tau+1}{2}} + C_0 \qquad (36)$$

where, $a = \min\{C_1, C_{21}, C_{22}, C_3\}$; $b = \min\{C_4, C_5, C_6\}$.

It follows from Lemma 2 that there is in finite time:

$$V(z) \leq \frac{C_0}{b-\lambda} \qquad (37)$$

where, $\lambda \in (0, b)$, set the time as:

$$T_r \leq \frac{1}{\lambda(1-\tau)}\ln\frac{V^{1-\tau}(t_0) + \frac{a}{\lambda}}{(\frac{C}{b(b-\lambda)})^{1-\tau} + \frac{a}{\lambda}} \qquad (38)$$

The constant term $C_0 = \sum_{i=1}^{2} \frac{1}{2\epsilon_{2i}} \bar{D}_i^2 + (1-\tau)(\frac{2}{\tau+1})^{-\frac{1+\tau}{1-\tau}}$. The second term is $(1-\tau)(\frac{2}{\tau+1})^{-\frac{1+\tau}{1-\tau}}$, which is a smaller constant when the constant τ is selected. The first item is $\sum_{i=1}^{2} \frac{1}{2\epsilon_{2i}} \bar{D}_i^2$, where in *Remark 1* $\bar{D}_i$ there is a detailed explanation, which is mainly related to lateral winds and the unmodeled part of the vehicle tires. Although these two parts cannot be accurately measured, their values are not particularly large when the vehicle is driving smoothly. The ϵ_{2i} is a design parameter that can be adjusted appropriately to make the first term smaller in value. Thus, although the constant term C_0 cannot be adjusted to be arbitrarily small, it can be kept within a small range. The function (36) conforms to the form of *Lemma 2* and therefore the system is practically finite time stability. From $V = V_1 + V_2 + V_3$ and (37), $\tilde{X}$, $\tilde{\lambda}_i$ and z_i are bounded. Hence $\xi_1 = z_1$ and $\xi_2 = z_2 + \eta_1$ are bounded. From (25) and (30), the virtual controller and actual controller are also bounded. Theorem 1 is proved.

The control method proposed in this paper is shown in Fig. 4. State observer (18) and disturbance observer (19) are designed to estimate the sideslip angle and the compound disturbance, and are used in the design of the controller. The virtual controller (25) is designed by redefining the path tracking error. Finally, the actual controller (28) is designed based on the backstepping method and the barrier Lyapunov function.

Remark 4: The methods proposed in this article mainly include state observer design and controller design. In the autonomous vehicle system, the sideslip angle is difficult to measure in practice, but it is necessary to know the sideslip angle in the control process. Therefore, a state observer is designed to estimate the sideslip angle, with the state variables β and γ. According to the relationship between autonomous vehicle system and reference path, the path tracking model is established, and the relationship between tracking error and autonomous vehicle system is derived. The controller design is based on the path tracing model with constraints on the state variables, which are e_p and $\dot{e}_p$.

Remark 5: The controller parameters are selected to meet the following requirements. Firstly, the state observer parameter design mainly focuses on choosing the appropriate matrix L so that the matrix H satisfies Herwitz at the same time making the state observer estimation the best. The k_1 and k_2 are the ranges of the constraints, and it is necessary to ensure that the target variables are always within the constraints, i.e., $k_1 > z_1, k_2 > z_2$. On this basis, since z_1 and z_2 are constantly changing during the path tracking process of the autonomous vehicle, slightly larger k_1 and k_2 should be chosen to ensure that $k_1 > z_1, k_2 > z_2$ are satisfied in the whole process. From the analysis results in (35), it can be viewed that the values of $\varrho_1, \varrho_2, \varsigma_1$ and ς_2 should be chosen largely as much as possible. The large values of control gains $\varrho_1, \varrho_2, \varsigma_1$ and ς_2 will improve the system performance. However, too large values of $\varrho_1, \varrho_2, \varsigma_1$ and ς_2 result in an aggressive control action. The design parameter $\tau \in$

$(0, 1)$, the smaller τ, the faster convergence rate of tracking error and the higher tracking accuracy. However, if the τ is too small, the system execution response cannot make the tracking error converge quickly, and instead will deteriorate the control effect.

IV. SIMULATION AND EXPERIMENTAL VERIFICATION
A. SIMULATION

In order to validate the effectiveness of the proposed method, MATLAB/Simulink is made to co-simulate with CarSim. The model of the proposed method is built in MATLAB/Simulink, and the C-class car in CarSim is chosen as the vehicle model, and the main parameters of the vehicle model are shown in Table. 1.

TABLE 1. Vehicle parameters.

Parameters	Values	Comments
m	1270kg	Vehicle mass
l_f	1.015m	Distance from center of mass to front wheel
l_r	1.895m	Distance from center of mass to rear wheel
I_z	1536.7kg·m²	Yaw inertia
C_f	55801N/rad	Lateral stiffness of front wheel
C_r	55801N/rad	Lateral stiffness of rear wheel

In order to validate the effectiveness of the proposed method in this paper, the commonly used double lane condition is selected. The lateral position of the reference path and the yaw angle are given by the following equations [35]:

$$
\begin{cases}
Y_d = \dfrac{d_{y1}}{2}[1 + \tanh(z_1)] - \dfrac{d_{y2}}{2}[1 + \tanh(z_2)] \\
\varphi_d = \arctan\left[d_{y1}\left(\dfrac{1}{\cosh(z_1)}\right)^2\left(\dfrac{1.2}{d_{x1}}\right)\right. \\
\left. -d_{y2}\left(\dfrac{1}{\cosh(z_2)}\right)^2\left(\dfrac{1.2}{d_{x2}}\right)\right]
\end{cases} \quad (39)
$$

where, $d_{x1} = d_{x2} = 25$, $z_1 = \frac{2.5}{25}(X - 68) - 1.2$, $z_2 = \frac{2.5}{25}(X - 133) - 1.2$, $d_{y1} = d_{y2} = 3.76$.

In order to verify the effectiveness of the method proposed in this paper under different conditions, two conditions are set. Case 1 is the road surface adhesion coefficient $\mu = 0.3$, vehicle speed $v_x = 48$km/h; Case 2 is the road surface adhesion coefficient $\mu = 1.0$, vehicle speed $v_x = 100$km/h.

In this section, three selected control methods are compared to illustrate the effectiveness of the method proposed in this paper. Since the simulation is in an ideal environment, there are no effects such as actuator delays, communication between devices, and so on. The parameters are adjusted according to the requirements in *Remark* 5 to improve the control accuracy as much as possible and get the best control effect. The selected control parameters are as follows:

Method I: This method is the one proposed in this paper. The parameters of Case 1 are set as: $x_p = 2$, $\tau = 8/11$, $k_1 = 10$; $k_2 = 10$; $\varrho_1 = 30$; $\varrho_2 = 30$; $\varsigma_1 = 12$; $\varsigma_2 = 12$; $\gamma_1 = 2.5$;
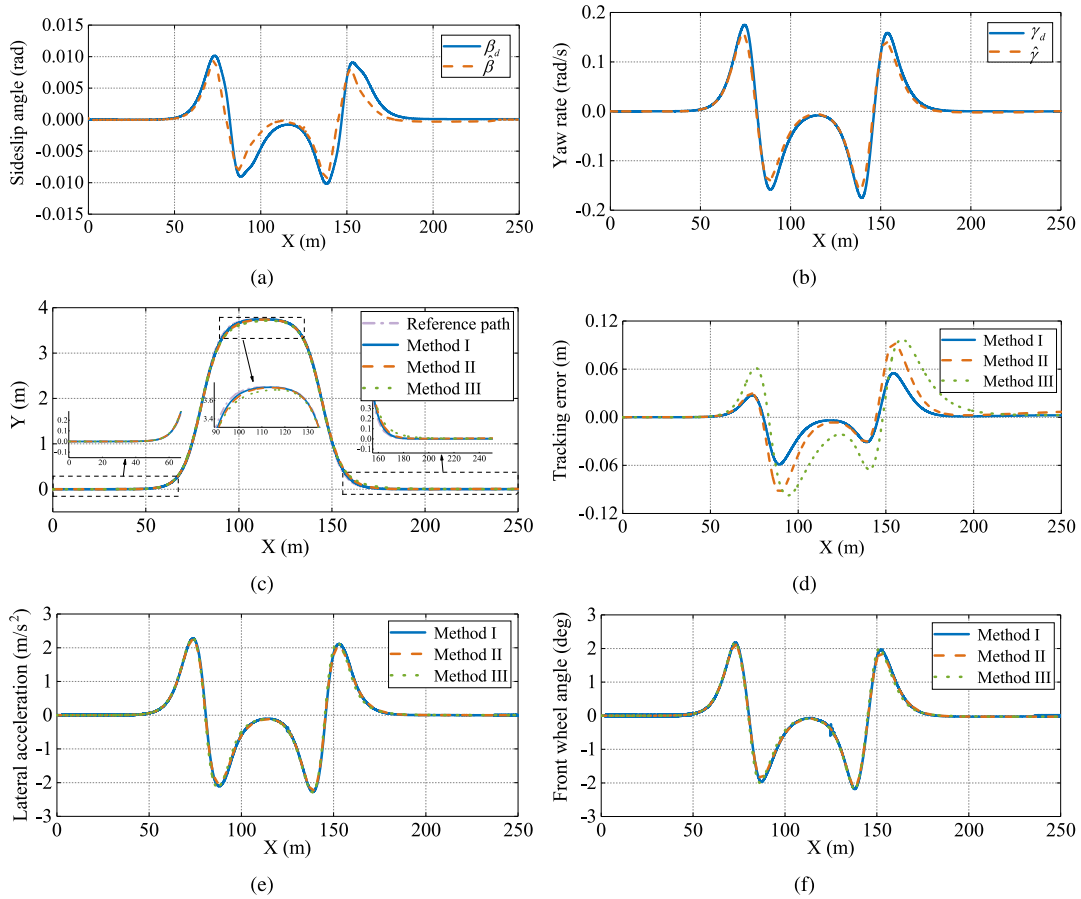
FIGURE 5. Simulation results of Case 1. (a) Estimation of sideslip angle; (b) Estimation of yaw rate; (c) Global path; (d) Tracking error; (e) Lateral acceleration; (f) Front wheel angle.

$\gamma_2 = 2.5$; $L = \begin{bmatrix} -0.5 & -0.6 \\ 0.9 & 1.3 \end{bmatrix}$. The parameters of Case 2 are set as: $x_p = 8$, $\tau = 8/11$, $k_1 = 10$; $k_2 = 10$; $\varrho_1 = 30$; $\varrho_2 = 30$; $\varsigma_1 = 12$; $\varsigma_2 = 12$; $\gamma_1 = 2.5$; $\gamma_2 = 2.0$; $L = \begin{bmatrix} -0.5 & -0.6 \\ 0.9 & 1.3 \end{bmatrix}$.

Method II: Based on method I, the finite time part is removed to design the virtual controller and the controller as:

$$\begin{cases} \eta_1 = -\varrho_1 z_1 - \dfrac{z_1}{2(k_1^2 - z_1^2)} \\ u = -\dfrac{1}{\zeta_3}(\zeta_1 + \hat{\zeta}_2 + x_p \hat{D}_2 - \dot{\eta}_1 + \varrho_2 z_2 + \dfrac{(k_2^2 - z_2^2)z_2}{2} \\ \quad + \dfrac{3z_2}{2(k_2^2 - z_2^2)}) \end{cases}$$

(40)

Method III: In order to reflect the effectiveness of the barrier Lyapunov function, the traditional backstepping control method is chosen for comparison and the controller is designed as:

$$u = -\dfrac{1}{\zeta_3}(\zeta_1 + \hat{\zeta}_2 + x_p \hat{D}_2 + \psi_1 \xi_2 + \psi_2(\xi_2 + \psi_1 \xi_1) + \xi_1)$$

(41)

B. SIMULATION RESULTS OF CASE 1

The simulation results of the three methods for Case 1 are shown in Fig. 5. To illustrate the effectiveness of the comparison method more intuitively, two performance indicators are introduced: 1) Root Mean Square Error (RMSE) RMSE $= \sqrt{\dfrac{1}{n} \sum_{i=1}^{n} e_i^2}$; 2) The maximum absolute value of error MAX $= \max_{i=1,\ldots,n}\{|e_i|\}$. The values of the two performance indicators for Case 1 are shown in Table. 2.

TABLE 2. The indicators for simulation Case 1.

Method	MAX	RMSE
Method I	0.0587	0.0185
Method II	0.0833	0.0299
Method III	0.0976	0.0394

Fig. 5(a) and 5(b) show the simulation results of the state observer. From Fig. 5(a), it can be seen that the estimates of sideslip angle and the reference sideslip angle have small errors and almost coincide at the end, and the estimation errors converge to near zero. From Fig. 5(b), it can be seen that the estimation of the yaw rate is very close to the reference yaw rate due to the yaw rate as a known variable, which indicates that the designed state observer has good
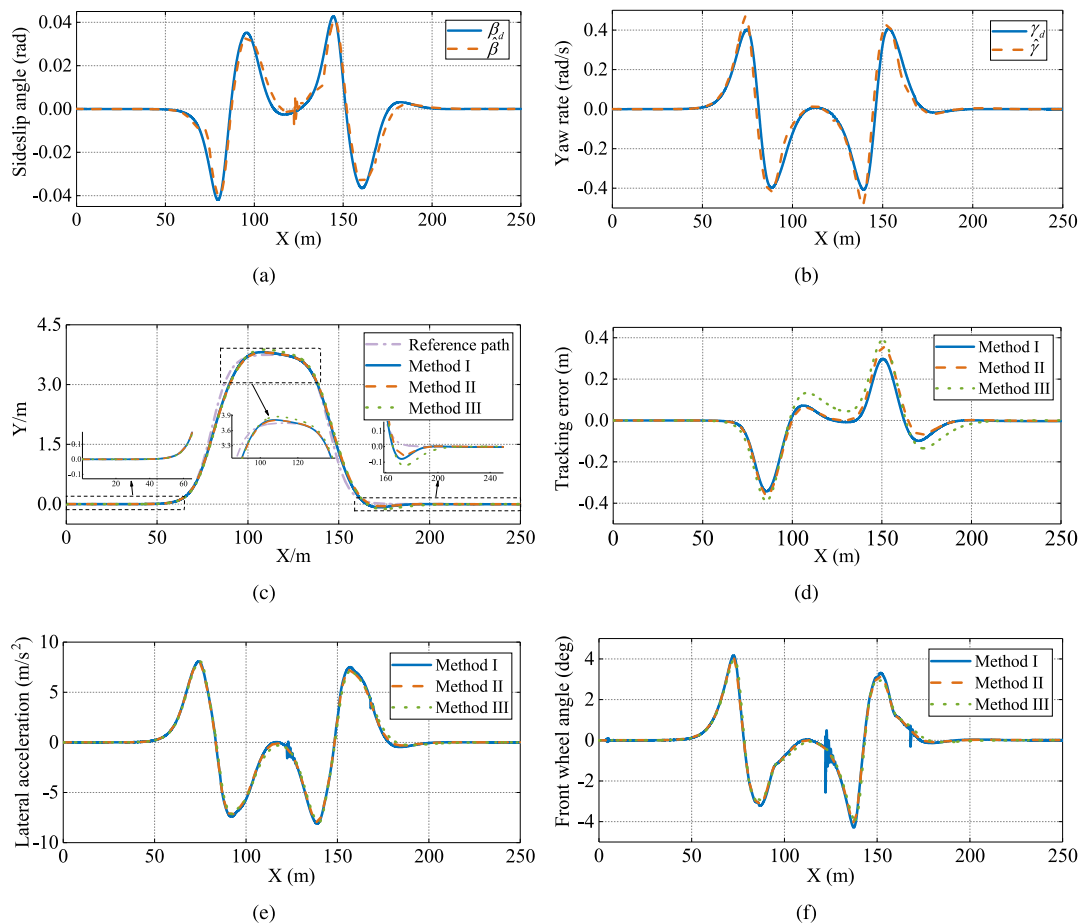
FIGURE 6. Simulation results of Case 2. (a) Estimation of sideslip angle; (b) Estimation of yaw rate; (c) Global path; (d) Tracking error; (e) Lateral acceleration; (f) Front wheel angle.

performance. From Fig. 5(c) and (d), it can be seen that all the three methods can track the reference path well and have smaller tracking errors throughout the tracking process, and the final tracking error converges to near zero. Combined with Table. 2, it can be seen that the absolute value of the maximum error of Method I is 0.0587m, which has better tracking effect than Method II and Method III. Fig. 5(e) and 5(f) show lateral acceleration and front wheel angle, respectively, from which it can be seen that the curves of three methods are very close to each other, indicating that the vehicle are in almost the same state at this time, and it is fair to compare the effectiveness of three methods. From Table. 2, it can be seen that the RMSE and MAX of Method I are smaller than those of Method II and Method III. Therefore, in simulation Case 1, Method I has better control effect.

C. SIMULATION RESULTS OF CASE 2

The simulation results of the three methods for Case 2 are shown in Fig. 6, and the values of two performance indicators for Case 2 are shown in Table. 3.

As can be seen from Fig. 6(a) and (b), the curves of the estimated sideslip angle and yaw rate fit the curves of the reference values well, indicating that the state observer also

TABLE 3. The indicators for simulation Case 2.

Method	MAX	RMSE
Method I	0.3430	0.0942
Method II	0.3606	0.1054
Method III	0.3880	0.1223

has good results in Case 2. From Fig. 6(c) and (d), it can be seen that all three methods can track the reference trajectory better, and finally the tracking error converges to near zero. However, compared with Case 1, the vehicle velocity is higher resulting in the tracking error will become larger. Combined with Table. 3, it can be seen that the absolute value of the maximum error of Method I is 0.3430m, and the RMSE of method I is smaller than that of Method II and Method III, which have better tracking results than Method II and Method III. From Fig. 6(e) and (f), it can be seen that the lateral acceleration and front wheel angle are in the same range, which indicates that the vehicle states of the three methods are almost the same. Under the same conditions, Method I has better control effect.

The above results show the simulation results in both cases and the simulation results show that Method I has
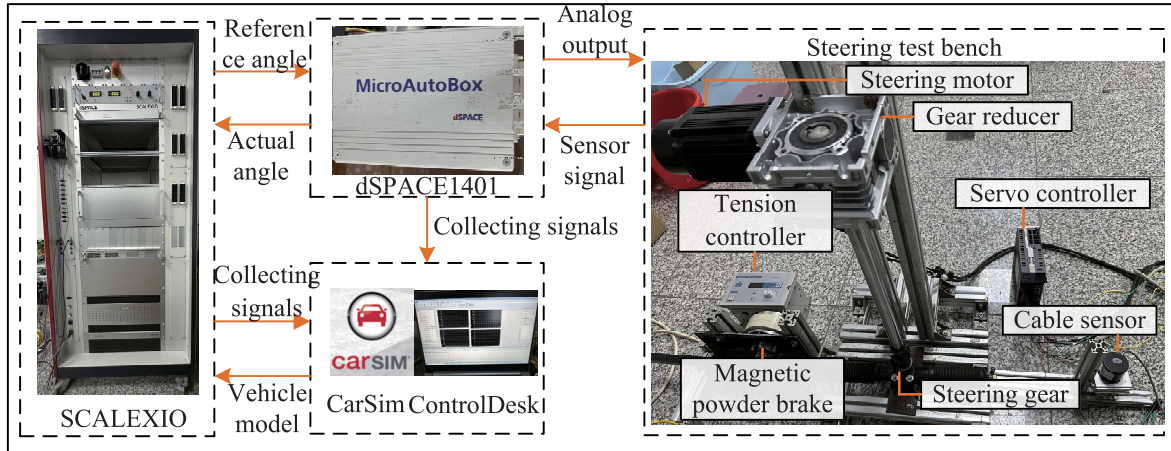
FIGURE 7. The schematic structure of the hardware-in-the-loop experiment.

better control performance. However, in the simulation validation as an ideal environment, the effects of sensor measurement noise, actuator response delay, and external disturbances on the control effect in the design environment are not taken into account. Therefore, in order to better validate the control effect of the proposed method in the real environment, hardware-in-the-loop experimental validation of the proposed method is performed.

D. HARDWARE IN THE LOOP EXPERIMENT

The schematic structure of the hardware-in-the-loop experiment is shown in Fig. 7.

It mainly includes steering test bench, SCALEXIO, dSPACE1401 and computer. The steering test bench is mainly composed of steering motor, gear reducer, servo controller, tension controller, magnetic powder brake, steering gear, cable sensor and table frame. During the experiment, the magnetic powder brake is controlled through the tension controller to simulate the road load in the real environment. The steering motor is controlled through the servo controller to drive the gear reducer and thus the steering gear to rotate. The displacement of the steering gear is collected by the tension sensor as the actual turning angle output. The computer with CarSim and ControlDesk is connected to SCALEXIO and dSPACE1401 via network. The control method is modelled in MATLAB/Simulink, the model is brushed into SCALEXIO with CarSim for code generation, and SCALEXIO sends the calculated desired corner to dSPACE1401 via CAN. The control model of the steering test rig is built in dSPACE1401 using MATLAB/Simulink, and the steering motor is controlled by using an analogue control servo controller based on the desired steering angle. The steering motor rotates and the steering displacement is captured by the tie wire sensor as the actual steering angle, which is input to dSPACE1401 through analogue signal acquisition. dSPACE1401 sends the actual steering angle to SCALEXIO through CAN communication to enable the vehicle to perform path tracking. The required signal data

is collected in ControlDesk to derive the actual effect of the control method. In order to compare the experimental results with the simulation results, the experimental environment settings and the simulation environment settings are kept the same.

Same as in the simulation verification, three methods are compared to illustrate the effectiveness of the proposed method, The hardware in the loop experiments are different from simulations. Although the vehicle model is still virtual, a steering test bench has been added. The latency of the steering actuator and the delay between controller communications need to be considered. As a result, the controller parameters are different from the simulation and cannot achieve the control accuracy in the simulation. On the basis of *Remark* 5 requirements, combined with the actual control effect, the parameters of Method I are set as follows:

**TABLE 4.** The indicators for experimental Case 1.

Method	MAX	RMSE
Method I	0.1567	0.0527
Method II	0.1862	0.0707
Method III	0.2733	0.1038

Method I: This method is the one proposed in this paper. The parameters of Case 1 are set as: $x_p = 3$, $\tau = 10/11$, $k_1 = 0.9$; $k_2 = 0.9$; $\varrho_1 = 8$; $\varrho_2 = 8$; $\varsigma_1 = 2$; $\varsigma_2 = 2$; $\gamma_1 = 1.5$; $\gamma_2 = 2.5$; $L = \begin{bmatrix} -0.5 & -0.6 \\ 0.9 & 1.3 \end{bmatrix}$. The parameters of Case 2 are set as: $x_p = 8$, $\tau = 10/11$, $k_1 = 0.9$; $k_2 = 0.9$; $\varrho_1 = 3$; $\varrho_2 = 3$; $\varsigma_1 = 2$; $\varsigma_2 = 2$; $\gamma_1 = 2.0$; $\gamma_2 = 1.5$; $L = \begin{bmatrix} -0.5 & -0.6 \\ 0.9 & 1.3 \end{bmatrix}$.

E. EXPERIMENTAL RESULTS OF CASE 1

The experimental results of the three methods for Case 1 are shown in Fig. 8. The values of the two performance indicators for Case 1 are shown in Table. 4.

Fig. 8(a) and 8(b) show the experimental results of the state observer designed in this paper. From Fig. 8(a), it can be seen
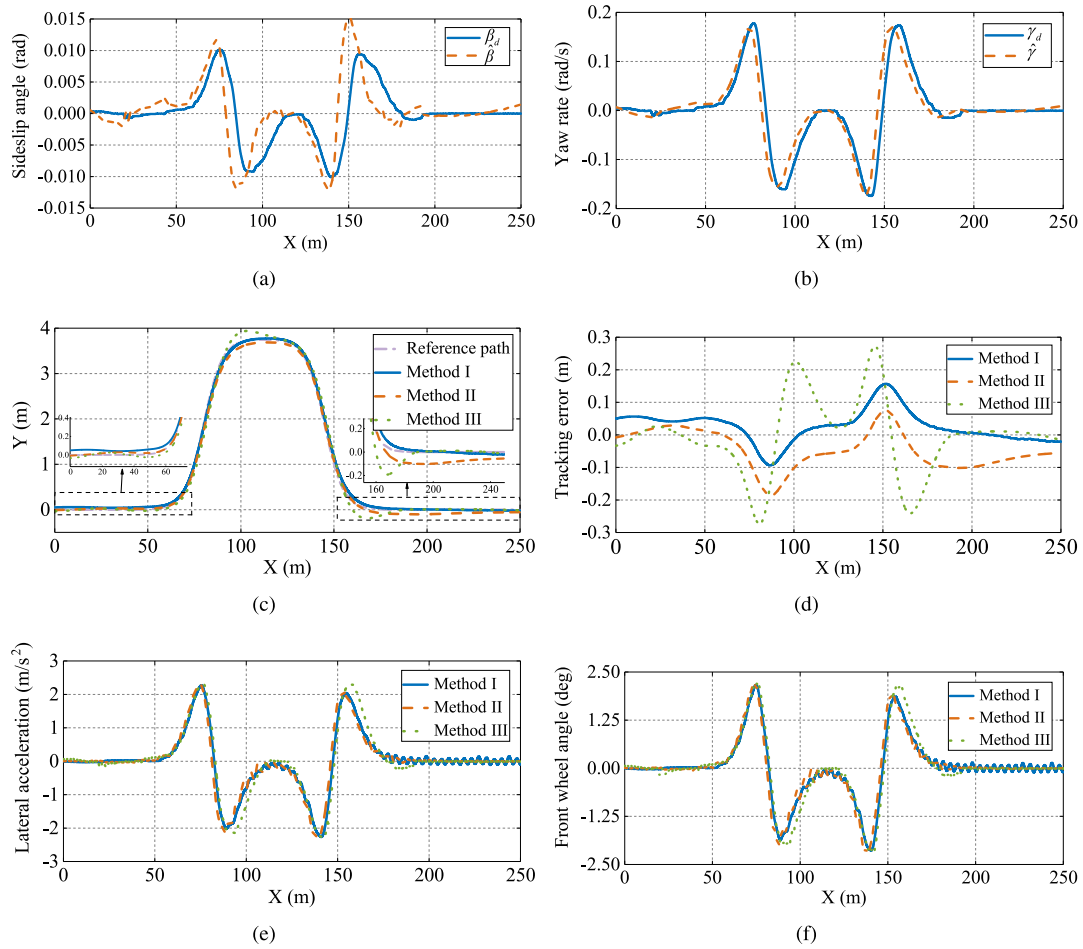
FIGURE 8. Experimental results of Case 1. (a) Estimation of sideslip angle; (b) Estimation of yaw rate; (c) Global path; (d) Tracking error; (e) Lateral acceleration; (f) Front wheel angle.

that the estimated curve of sideslip angle can fit well with the reference sideslip angle curve. Although there is a certain difference between the estimated value of the sideslip angle and the value of the sideslip angle, the estimation effect is not very satisfactory considering that in the hardware-in-the-loop experiments, the estimation effect will be interfered by other factors, such as sensor noise and steering clearance. Therefore, overall, the estimation of the sideslip angle can meet the requirements of path tracking control. As can be seen from Fig. 8(b), since the yaw rate is a known variable, the error between its estimated value and the reference value is very small, which also indicates the effectiveness of the state observer designed in this paper. From Fig. 8(c) and 8(d), it can be seen that all the three methods are able to track the reference path well during the path tracking process. At longitudinal positions 0-50m and 200-250m, the sensor noise and the existence of certain gaps in the steering test bed prevented the full output of 0 degree of steer, which prevented all three methods from fully converging to zero at the start of tracking as well as at the end of tracking error. Combined with Table. 4, it can be seen that the maximum tracking error of Method I has an absolute value of 0.1567m, which has a

better tracking effect compared to Method II and Method III. From Fig. 8(e) and 8(f), it can be seen that the values of lateral acceleration and front wheel angle are within the same range for all three methods, with a small chatting in the front wheel angle in the second half of the tracking due to a slightly larger change in the amount of control for Method I. As can be seen from Table. 4, RMSE and MAX of Method I are smaller than those of Methods II and III. Therefore, in general under the experimental condition of working Case 1, the path tracking control effect of method I is better than that of Method II and method III.

F. EXPERIMENTAL RESULTS OF CASE 2

The experimental results of the three methods for Case 2 are shown in Fig. 9, and the values of two performance indicators for Case 2 are shown in Table. 5.

Fig. 9(a) and 9(b) show the experimental results of the state observer under Case 2. From Fig. 9(a), it can be seen that the sideslip angle estimation curve as a whole can follow the reference sideslip angle curve well, but there is a large abrupt change at the longitudinal position around 130 m, and then returns to normal. The same trend is observed in the
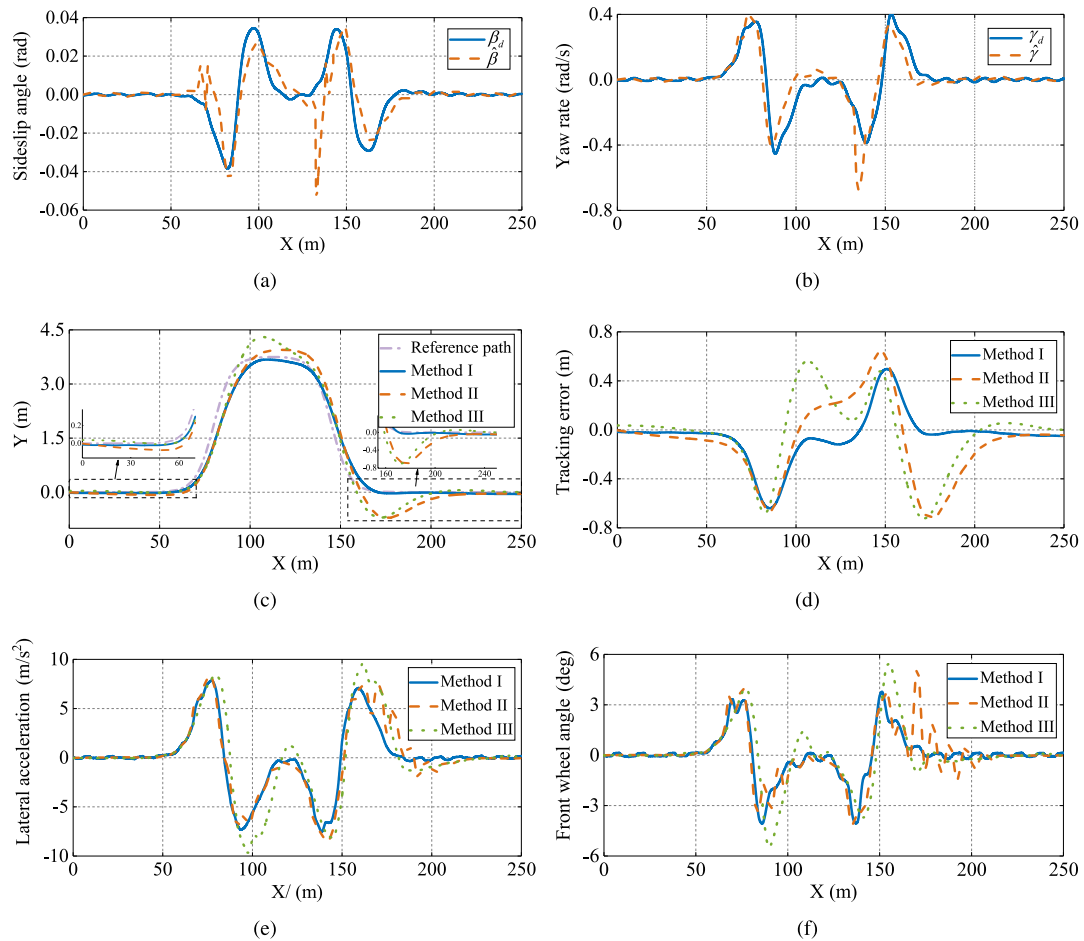
FIGURE 9. Experimental results of Case 2. (a) Estimation of sideslip angle; (b) Estimation of yaw rate; (c) Global path; (d) Tracking error; (e) Lateral acceleration; (f) Front wheel angle.

TABLE 5. The indicators for experimental Case 2.

Method	MAX	RMSE
Method I	0.6395	0.1836
Method II	0.7042	0.2470
Method III	0.7724	0.2899

estimation of yaw rate in Fig. 9(b), which has a small effect on the control effectiveness. Therefore, the state observer designed in this paper has well results at high velocity as well. From Fig. 9(c) and 9(d), it can be seen that all the three methods are able to track the reference path well during the path tracking process. Similar to the case in Case 1, at the beginning and end of the path tracking due to the limitations of the hardware equipment, it is not possible to make the error completely converge to zero. Combined with Table. 5, it can be seen that the maximum tracking error of Method I has an absolute value of 0.6395m, which has a better tracking effect compared to Method II and Method III. From Fig. 9(e) and 9(f), it can be seen that the values of lateral acceleration and front wheel angle are in the same range for all three methods. Due to the high velocity of

the vehicle in Case 2, the lateral acceleration of the three methods is high, but the vehicle is still stable for path tracking. Due to the high velocity of the vehicle, the response of the steering test bed could not be achieved without delay in the pure simulation environment, and had a certain delay, which led to different degrees of jerks in the front wheel angle for all three methods, especially more obvious after 150m in the longitudinal position. As can be seen from Table. 5, the RMSE and MAX of Method I are smaller than those of Methods II and III. Therefore, in general under the simulation condition of working condition two, the path tracking control effect of method one is better than that of method II and method III.

In summary it is stated that under the same experimental conditions, no matter low-velocity and high-velocity working conditions, the method proposed in this paper is able to complete the path tracking control with better control effect. As can be seen in Fig. 5(c) and Fig. 6(c), after 150m in the longitudinal position, the vehicle enters the last curve subsequently travelling in a straight line, and the tracking error should converge to zero. Method I has finite time control compared to Method II. From Fig. 5 (d) and Fig. 6 (d),

it can be seen that Method I has smaller tracking error and can converge to zero faster after a longitudinal position of 150m. Since it is an ideal environment in the simulation and the actuator delay is not taken into account, the hardware-in-the-loop experiments under the same conditions show the advantage of finite time more clearly, as shown in Fig. 8(d) and Fig. 9(d). The above simulations and hardware-in-the-loop experiments illustrate that the addition of finite-time control significantly improves the tracking accuracy as well as the convergence rate.

V. CONCLUSION

In this paper, a state-constrained finite-time path tracking controller is proposed for the path tracking problem of autonomous vehicle affected by compound disturbance and unmeasurable variables. Since the sideslip angle is difficult to measure in practice, a state observer is designed for estimation to improve the accuracy of the model. A disturbance observer is designed to estimate the disturbance to the vehicle, including side wind and tire force changes, to improve the path tracking accuracy and stability. The combination of backstepping, finite time convergence technique and barrier Lyapunov function ensures that the system state converges in finite time and is proved based on Lyapunov stability theory. Finally, simulation and hardware-in-the-loop experimental results demonstrate the effectiveness of the proposed method.

The barrier Lyapunov designed in this paper is a logarithmic function, and in the future, we will explore how the tangent type function can solve the constrained and unconstrained cases at the same time, and how to apply it to the path tracking of the autonomous vehicle will be one of our future research directions. In addition, this paper does not consider the steering-by-wire system in the autonomous vehicle path tracking problem. However, in practice, autonomous vehicle will inevitably experience faulty situations (e.g., steering motor loss of effectiveness, stuck, and outage etc). Fault-tolerant control [36] research for faulty situations will be part of our subsequent work.

REFERENCES

[1] H. Wang, Y. Huang, A. Khajepour, D. Cao, and C. Lv, "Ethical decision-making platform in autonomous vehicles with lexicographic optimization based model predictive controller," *IEEE Trans. Veh. Technol.*, vol. 69, no. 8, pp. 8164–8175, Aug. 2020.

[2] R. Rajamani, C. Zhu, and L. Alexander, "Lateral control of a backward driven front-steering vehicle," *Control Eng. Pract.*, vol. 11, no. 5, pp. 531–540, May 2003.

[3] N. R. Kapania and J. C. Gerdes, "Design of a feedback-feedforward steering controller for accurate path tracking and stability at the limits of handling," *Vehicle Syst. Dyn.*, vol. 53, no. 12, pp. 1687–1704, Dec. 2015.

[4] R. Marino, S. Scalzi, and M. Netto, "Design of a feedback-feedforward steering controller for accurate path tracking and stability at the limits of handling," *Control Eng. Pract.*, vol. 19, no. 12, pp. 1459–1467, Dec. 2011.

[5] J. Guo, P. Hu, L. Li, and R. Wang, "Design of automatic steering controller for trajectory tracking of unmanned vehicles using genetic algorithms," *IEEE Trans. Veh. Technol.*, vol. 61, no. 7, pp. 2913–2924, Sep. 2012.

[6] J. Chen, Z. Shuai, H. Zhang, and W. Zhao, "Path following control of autonomous four-wheel-independent-drive electric vehicles via second-order sliding mode and nonlinear disturbance observer techniques," *IEEE Trans. Ind. Electron.*, vol. 68, no. 3, pp. 2460–2469, Mar. 2021.

[7] C. Hu, H. Jing, R. Wang, and F. Yan, "Robust H_∞ output-feedback control for path following of autonomous ground vehicles," *Mech. Syst. Signal Process.*, vol. 70, pp. 414–427, Mar. 2016.

[8] Y. Rasekhipour, A. Khajepour, S.-K. Chen, and B. Litkouhi, "A potential field-based model predictive path-planning controller for autonomous road vehicles," *IEEE Trans. Intell. Transp. Syst.*, vol. 18, no. 5, pp. 1255–1267, May 2017.

[9] S. Ding, L. Liu, and W. X. Zheng, "Sliding mode direct yaw-moment control design for in-wheel electric vehicles," *IEEE Trans. Ind. Electron.*, vol. 64, no. 8, pp. 6752–6762, Aug. 2017.

[10] P. Falcone, H. Eric Tseng, F. Borrelli, J. Asgari, and D. Hrovat, "MPC-based yaw and lateral stabilisation via active front steering and braking," *Vehicle Syst. Dyn.*, vol. 46, no. sup1, pp. 611–628, Sep. 2008.

[11] P. Falcone, F. Borrelli, H. E. Tseng, J. Asgari, and D. Hrovat, "Linear time-varying model predictive control and its application to active steering systems: Stability analysis and experimental validation," *Int. J. Robust Nonlinear Control*, vol. 18, no. 8, pp. 862–875, May 2008.

[12] G. Chen, J. Yao, H. Hu, Z. Gao, L. He, and X. Zheng, "Design and experimental evaluation of an efficient MPC-based lateral motion controller considering path preview for autonomous vehicles," *Control Eng. Pract.*, vol. 123, Jun. 2022, Art. no. 105164.

[13] Z. Zhang, L. Zheng, Y. Li, S. Li, and Y. Liang, "Cooperative strategy of trajectory tracking and stability control for 4WID autonomous vehicles under extreme conditions," *IEEE Trans. Veh. Technol.*, vol. 72, no. 3, pp. 3105–3118, Mar. 2023.

[14] X. Ji, X. He, C. Lv, Y. Liu, and J. Wu, "Adaptive-neural-network-based robust lateral motion control for autonomous vehicle at driving limits," *Control Eng. Pract.*, vol. 76, pp. 41–53, Jul. 2018.

[15] Y. Wang, Y. Liu, Y. Wang, and T. Chai, "Neural output feedback control of automobile steer-by-wire system with predefined performance and composite learning," *IEEE Trans. Veh. Technol.*, vol. 72, no. 5, pp. 5906–5921, May 2023.

[16] Y. Wang, Y. Wang, and M. Tie, "Hybrid adaptive learning neural network control for steer-by-wire systems via sigmoid tracking differentiator and disturbance observer," *Eng. Appl. Artif. Intell.*, vol. 104, Sep. 2021, Art. no. 104393.

[17] Y. Wang, Y. Wang, and G. Chen, "Robust composite adaptive neural network control for air management system of PEM fuel cell based on high-gain observer," *Neural Comput. Appl.*, vol. 32, no. 14, pp. 10229–10243, Jul. 2020.

[18] Y. Wang, Y. Liu, J. Ding, and D. Wang, "Adaptive type-2 fuzzy output feedback control using nonlinear observers for permanent magnet synchronous motor servo systems," *Eng. Appl. Artif. Intell.*, vol. 131, May 2024, Art. no. 107833.

[19] J. Zhang, S. Wang, P. Zhou, L. Zhao, and S. Li, "Novel prescribed performance-tangent barrier Lyapunov function for neural adaptive control of the chaotic PMSM system by backstepping," *Int. J. Electr. Power Energy Syst.*, vol. 121, Oct. 2020, Art. no. 105991.

[20] Y. Song, Y. Xia, J. Wang, J. Li, C. Wang, Y. Han, and K. Xiao, "Barrier Lyapunov function-based adaptive prescribed performance control of the PMSM used in robots with full-state and input constraints," *J. Vib. Control*, vol. 29, nos. 5–6, pp. 1400–1416, Mar. 2023.

[21] M. Zou, J. Yu, Y. Ma, L. Zhao, and C. Lin, "Command filtering-based adaptive fuzzy control for permanent magnet synchronous motors with full-state constraints," *Inf. Sci.*, vol. 518, pp. 1–12, May 2020.

[22] S. P. Bhat and D. S. Bernstein, "Lyapunov analysis of finite-time differential equations," in *Proc. Amer. Control Conf.*, vol. 3, 1995, pp. 1831–1832.

[23] Y. Liu, D. Yao, L. Wang, and S. Lu, "Distributed adaptive fixed-time robust platoon control for fully heterogeneous vehicles," *IEEE Trans. Syst., Man, Cybern., Syst.*, vol. 53, no. 1, pp. 264–274, Jan. 2023.

[24] L. Cao, Z. Cheng, Y. Liu, and H. Li, "Event-based adaptive NN fixed-time cooperative formation for multiagent systems," *IEEE Trans. Neural Netw. Learn. Syst.*, vol. 35, no. 5, pp. 6467–6477, May 2024.

[25] D. Cui, C. K. Ahn, and Z. Xiang, "Fault-tolerant fuzzy observer-based fixed-time tracking control for nonlinear switched systems," *IEEE Trans. Fuzzy Syst.*, vol. 31, no. 12, pp. 4410–4420, Dec. 2023.

[26] H. Deng and M. Krstić, "Stochastic nonlinear stabilization—I: A backstepping design," *Syst. Control Lett.*, vol. 32, no. 3, pp. 143–150, Nov. 1997.

[27] B. Chen and C. Lin, "Finite-time stabilization-based adaptive fuzzy control design," *IEEE Trans. Fuzzy Syst.*, vol. 29, no. 8, pp. 2438–2443, Aug. 2021.

[28] L. Wang, H. Wang, P. X. Liu, S. Ling, and S. Liu, "Fuzzy finite-time command filtering output feedback control of nonlinear systems," *IEEE Trans. Fuzzy Syst.*, vol. 30, no. 1, pp. 97–107, Jan. 2022.

[29] J. Ma, J. H. Park, and S. Xu, "Command-filter-based finite-time adaptive control for nonlinear systems with quantized input," *IEEE Trans. Autom. Control*, vol. 66, no. 5, pp. 2339–2344, May 2021.

[30] J. Yu, P. Shi, and L. Zhao, "Finite-time command filtered backstepping control for a class of nonlinear systems," *Automatica*, vol. 92, pp. 173–180, Jun. 2018.

[31] Y.-X. Li, "Finite time command filtered adaptive fault tolerant control for a class of uncertain nonlinear systems," *Automatica*, vol. 106, pp. 117–123, Aug. 2019.

[32] A. Francesco, A. Marco, and D. Peter, "Finite-time control of linear systems subject to parametric uncertainties and disturbances," *Automatica*, vol. 37, no. 9, pp. 1459–1463, Sep. 2001.

[33] D. Cui, C. K. Ahn, Y. Sun, and Z. Xiang, "Mode-dependent state observer-based prescribed performance control of switched systems," *IEEE Trans. Circuits Syst. II, Exp. Briefs*, vol. 71, no. 8, pp. 3810–3814, Aug. 2024.

[34] M. M. Zirkohi, "Command filtering-based adaptive control for chaotic permanent magnet synchronous motors considering practical considerations," *ISA Trans.*, vol. 114, pp. 120–135, Aug. 2021.

[35] P. Falcone, F. Borrelli, J. Asgari, H. E. Tseng, and D. Hrovat, "Predictive active steering control for autonomous vehicle systems," *IEEE Trans. Control Syst. Technol.*, vol. 15, no. 3, pp. 566–580, May 2007.

[36] D. Cui, B. Niu, D. Yang, T. Hayat, and F. E. Alsaadi, "Adaptive neural fault-tolerant control for a class of stochastic switched nonlinear systems," *IEEE Access*, vol. 7, pp. 93219–93228, 2019.

SUCAI ZHANG received the B.S. degree in vehicle engineering from Guilin University of Aerospace Technology, Guilin, China, in 2019, and the M.S. degree in vehicle engineering from Liaoning University of Technology, Jinzhou, China, in 2022. He is currently pursuing the Ph.D. degree in mechanical engineering with Northeastern University, Shenyang, China.

He has authored or co-authored five journals and conference papers. His research interests include intelligent control of nonlinear systems and intelligent control of vehicles.

PENGXIANG LI received the B.S. degree in engineering from Ningxia Institute of Science and Technology, in 2012, and the M.S. degree in mechanical engineering from Northeastern University, Shenyang, China, in 2019.

Since 2019, he has been a Lecturer with Ningxia Institute of Technology, mainly focusing on the management of new energy vehicles and battery energy storage systems. He is currently a Teacher of the Dual Teacher Practice and Exercise Program Project of Ningxia Hui Autonomous Region, and a Domestic Visiting Scholar of young backbone teachers in higher education institutions in the central and western part of China, Northeastern University. He hosted one Ningxia Natural Science Foundation Project, two education reform projects, one autonomous region collaborative education project, published four articles, and obtained four patents.

Mr. Li won one third prize in teaching achievements in autonomous region and was honored as an excellent guiding teacher in the vocational college skills competition in the whole region. He guided students to win more than 20 awards in subject competitions.

YAN LIU received the B.S. degree in vehicle engineering from Dalian Jiaotong University, Dalian, China, in 2016, and the M.S. and Ph.D. degrees in vehicle engineering from Northeastern University, Shenyang, China, in 2018 and 2023, respectively.

He is currently the Director of the Vehicle Engineering Department, School of Automotive and Transportation Engineering, Liaoning University of Technology. He has authored or co-authored more than ten journals and conference papers. His research interests include intelligent control of nonlinear systems, servo motor control, and intelligent control of vehicles.

• • •